

## Geometry of the Nojima Fault at Nojima-Hirabayashi, Japan – II. Microstructures and their Implications for Permeability and Strength

DIANE E. MOORE,<sup>1</sup> DAVID A. LOCKNER,<sup>1</sup> HISAO ITO,<sup>2,3</sup> RIUJI IKEDA,<sup>4,5</sup> HIDEKI TANAKA,<sup>6,7</sup> and  
KENTARO OMURA<sup>8</sup>

*Abstract*—Samples of damage-zone granodiorite and fault core from two drillholes into the active, strike-slip Nojima fault zone display microstructures and alteration features that explain their measured present-day strengths and permeabilities and provide insight on the evolution of these properties in the fault zone. The least deformed damage-zone rocks contain two sets of nearly perpendicular (60–90° angles), roughly vertical fractures that are concentrated in quartz-rich areas, with one set typically dominating over the other. With increasing intensity of deformation, which corresponds generally to increasing proximity to the core, zones of heavily fragmented rock, termed microbreccia zones, develop between prominent fractures of both sets. Granodiorite adjoining intersecting microbreccia zones in the active fault strands has been repeatedly fractured and locally brecciated, accompanied by the generation of millimeter-scale voids that are partly filled with secondary minerals. Minor shear bands overprint some of the heavily deformed areas, and small-scale shear zones form from the pairing of closely spaced shear bands. Strength and permeability measurements were made on core collected from the fault within a year after a major (Kobe) earthquake. Measured strengths of the samples decrease regularly with increasing fracturing and fragmentation, such that the gouge of the fault core and completely brecciated samples from the damage zone are the weakest. Permeability increases with increasing disruption, generally reaching a peak in heavily fractured but still more or less cohesive rock at the scale of the laboratory samples. Complete loss of cohesion, as in the gouge or the interiors of large microbreccia zones, is accompanied by a reduction of permeability by 1-2 orders of magnitude below the peak values. The core samples show abundant evidence of hydrothermal alteration and mineral precipitation. Permeability is thus expected to decrease and strength to increase somewhat in active fault strands between earthquakes, as mineral deposits progressively seal fractures and fill pore spaces.

**Key words:** Fault zone, microstructures, secondary mineralization, permeability, strength.

---

<sup>1</sup> U. S. Geological Survey, Menlo Park, CA , USA. E-mail: dmoore@usgs.gov

<sup>2</sup> Geological Survey of Japan, Tsukuba, Japan.

<sup>3</sup> Center for Deep Earth Exploration, Japan Agency for Marine-Earth Science and Technology, Yokohama, Japan.

<sup>4</sup> National Research Institute for Earth Science and Disaster Prevention, Tsukuba, Japan.

<sup>5</sup> Department of Earth and Planetary Sciences, Hokkaido University, Hokkaido, Japan.

<sup>6</sup> Ehime University, Matsuyama, Japan.

<sup>7</sup> Department of Earth and Planetary Sciences, University of Tokyo, Tokyo, Japan.

<sup>8</sup> National Research Institute for Earth Science and Disaster Prevention, Tsukuba, Japan.

## 1. Introduction

Most of our information regarding the internal structure of fault zones comes from the study of ancient, exhumed faults whose microscopic-scale textures may have suffered post-faulting thermal, chemical, and deformational overprints. Thus, it was especially significant that, within a year following the January, 1995 Kobe (Hyogo-ken Nanbu) earthquake in Japan, the Geological Survey of Japan (GSJ) and the National Research Institute for Earth Science and Disaster Prevention (NIED) began drilling programs into the Nojima fault zone, which ruptured during the earthquake. One of the principal goals of both groups was the recovery of core to allow petrographic, chemical, and physical examination of an active fault zone at depth immediately after an earthquake.

The results of permeability and strength tests conducted on core samples from both drillholes are reported by LOCKNER *et al.* (this volume, hereinafter cited as paper I). An essential part of any laboratory study is to place the measured physical properties of the samples in the context of their microstructures and mineral assemblages. In this paper, we provide an overview of the brittle deformation and secondary mineralization features of the core samples, illustrating how these processes compete to influence strength and permeability.

## 2. Tectonic Setting of the Nojima Fault

The approximately 8-km long Nojima fault parallels the northwest coastline of Awaji Island, located in Osaka Bay about 4 km southwest of the city of Kobe, Japan (Fig. 1 of paper I). The Nojima fault is a right-lateral strike-slip fault with a reverse component (MIZUNO *et al.*, 1990) that strikes N35-40°E and dips about 83° to the southeast (e.g., TANAKA *et al.*, 2001). The fault cuts the Cretaceous (66-88 Ma; TAKAHASHI, 1992) Nojima granodiorite (Fig. 1 of paper I) at depth. Recent activity on the Nojima fault may have begun about 1.2 Ma, associated with uplift of Awaji Island (MURATA *et al.*, 2001), however, the present-day Nojima fault may have reactivated a much older, exhumed fault. MURAKAMI and TAGAMI (2004) reported a cooling age of 56 Ma for pseudotachylyte from surface exposures of the fault (OTSUKI *et al.*, 2003), based on fission track thermochronologic analysis of zircons. They concluded that the pseudotachylyte was generated at depths of about 8-12 km (see also TAGAMI and MURAKAMI, 2007; TANAKA *et al.*, 2007). Deformation textures in older, foliated cataclasites estimated to have formed between 5 and 10 km depth indicate right-lateral offset with some vertical component (LIN *et al.*, 2001), the same as observed on the fault today.

Surface offset associated with the Hyogo-ken Nanbu (Kobe) earthquake of January 17, 1995 was concentrated on the Nojima fault and some adjoining faults at its southwest termination (Fig. 1 of paper I) (AWATA *et al.*, 1996; LIN and UDA, 1996). Maximum net slip of 2.15 m was measured near the GSJ and NIED drillholes; this net slip resolves into 1.8 m right-lateral offset and 1.3 m reverse motion with east side up (LIN and UDA, 1996).

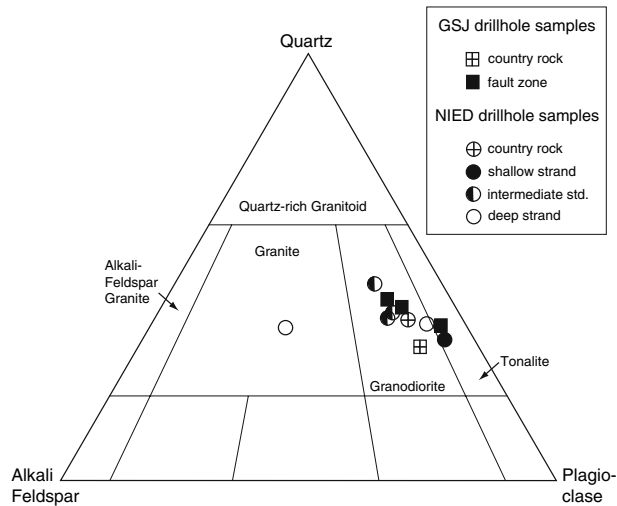


Figure 1

Classification of 11 core samples with well-preserved igneous textures, using the plutonic-rock classification scheme of STRECKEISEN (1974).

An earthquake recurrence interval of about 2000 years has been estimated from trenching studies (AWATA and SUZUKI, 1996). Based on measurements of borehole breakouts (IKEDA *et al.*, 2001) and deformation rate analysis of core samples (YAMAMOTO *et al.*, 2000), the maximum horizontal compression direction in the two drillholes is presently NW-SE ( $N49^{\circ}W \pm 15^{\circ}$ , IKEDA *et al.*, 2001), nearly perpendicular to the strike of the fault. YAMAMOTO *et al.* (2000) noted that this orientation is consistent with the contraction measured over the past 100 years in the Osaka Bay region by the Geographical Survey Institute of Japan. Throughout much of the Quaternary Period, however, the southwestern part of Japan was characterized by E-W compression (e.g., SENO, 1999).

### 3. Scope of Study

The borehole drilled by the GSJ 75 m to the SE of the surface trace crossed a gouge-bearing fault at about 624 m measured depth, whereas the one drilled by the NIED 302 m to the SE of the fault crossed three possible fault strands at depths of about 1140 m, 1312 m, and 1800 m (Fig. 2 of paper I). Core samples from all four fault strands were obtained for laboratory measurements of strength and permeability, as detailed in paper I. A polished thin section was prepared from each sample for petrographic examination. All but two of the thin sections are oriented perpendicular to the axis of the core. Because the maximum deviation of both boreholes from vertical was about  $6\text{--}7^{\circ}$  (IKEDA, 2001; TANAKA *et al.*, 2001), these thin sections are oriented nearly horizontally. The two exceptions are

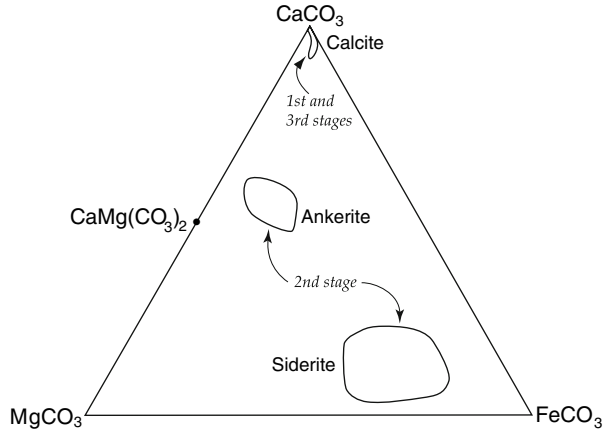


Figure 2

Compositions of carbonate minerals in Nojima fault core samples, obtained by electron microprobe techniques. Trace amounts of stage 2 dolomite, containing only about 5% substitution of Fe for Mg, were also found.

gouge samples NIED 81-22A and GSJ 99-4 which, owing to their small size, were cut parallel to the cylinder axis. The thin-section set, listed in Table 1, includes an example of the granitic country rock from shallow depths in each drillhole, although the GSJ country-rock sample was not tested by LOCKNER *et al.* The other samples are classified as damage zone or fault core, following the usage of CHESTER and LOGAN (1986; see also CHESTER *et al.*, 1993, and CAINE *et al.*, 1996). A fault core was not identified in the deepest fault strand intersected by the NIED drillhole.

This petrographic study is largely based on transmitted- and reflected-light microscopy. Additional observations were made with a scanning electron microscope (SEM) equipped with a high-resolution backscattered electron detector and an energy dispersive X-ray spectrometer (EDX) for qualitative determinations of element abundances. Compositions of carbonate minerals were obtained using electron microprobe techniques, with carbonate-mineral standards. Three sets of point counts were made with the aid of a mechanical stage, with a 1 mm × 1 mm grid. Point-count totals for the variably sized samples range from 530 to 1001. Because the core was not oriented, the relative orientations of microstructures in a given thin section were measured with reference to a designated 0° azimuth parallel to the long dimension of the thin section.

#### 4. Petrographic Observations

##### 4.1. Igneous and Secondary Mineral Assemblages

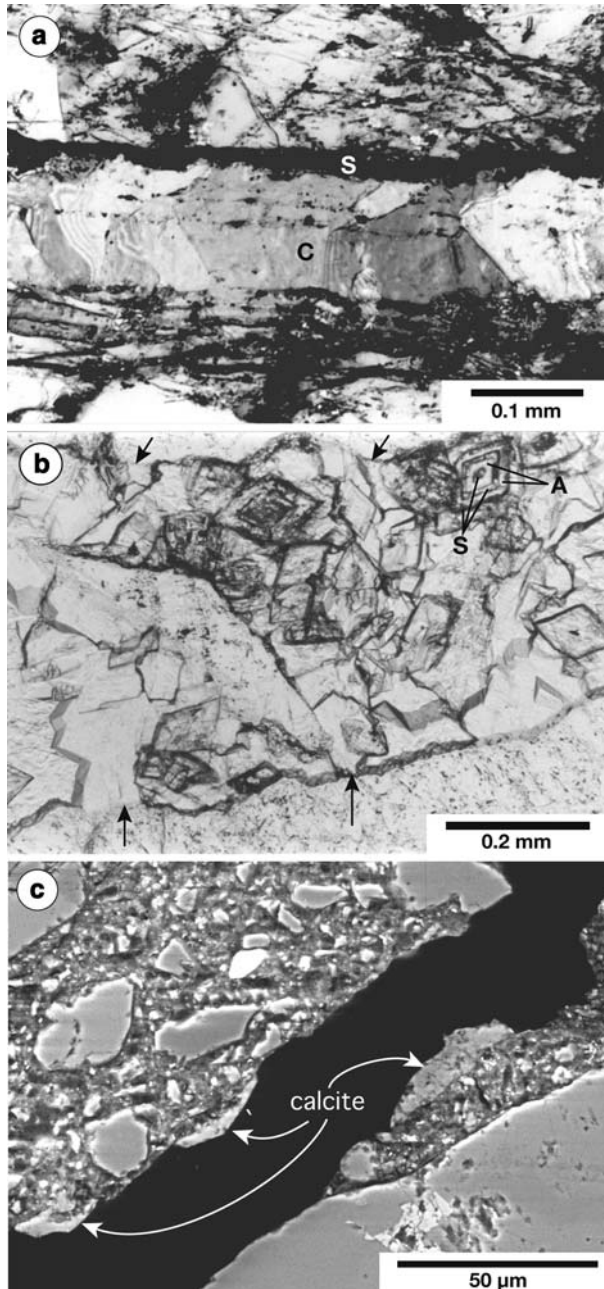
Igneous mineral modes were obtained from point counts of 11 samples with reasonably well preserved igneous textures. In the less deformed samples, it usually is

Table 1  
*Samples examined in this study*

<u>Sample #</u>	<u>Depth (m)</u>	<u>≈ Horiz. Dist. from Gouge Core* (m)</u>	<u>Description</u>	<u>% Secondary Minerals</u>	<u>% Disrupted (see text)</u>
<u>GSJ Drillhole</u>					
258.6	258.6		country rock; relict amphiboles	17	20
74-17	503.4	14.5	damage zone; 4 mm-wide microbreccia zone	44	40
91-6	582.0	5.0	damage zone; 10 mm-wide microbreccia zone	37	72
98-31	623.6	0	core; coarse-grained, foliated gouge (Type I**)	N A	100
99-4	624.4	0	core; fine-grained gouge (Type II**)	N A	100
101-2	634.1	1.1	damage zone; two ≤ 6 mm-wide shears	38 [36-41]	64
118-21	730.4	12.7	damage zone; dilational fractures, relict amph.	19	20
<u>NIED Drillhole</u>					
12-1A	659.3		country rock; relict amphiboles	5	2
<u>Shallow strand:</u>					
32-20	1063.7	18.0	damage zone; wide veins, minor brecciation	46	45
34-27	1077.9	14.5	damage zone; microbreccia zones	61 [55-64]	56
43-37-1	1131.8	2.0	damage zone; minor shear	36	70
45-23	1140.1	0	core; fine-grained gouge (Type II)	N A	100
<u>Intermediate strand:</u>					
74-19	1278.6	7.5	damage zone; dilational fractures	18	12
76-17	1289.0	5.0	damage zone; 20 mm-wide microbreccia zone	N A	77
80-29	1307.5	1.0	damage zone; dilational fractures	26	18
81-22A	1312.0	0	core; coarse-grained, foliated gouge (Type I)	N A	100
82-40	1320.3	2.0	damage zone; incipient shears	22 [18-35]	60
85-15B	1332.2	5.0	damage zone; large microbreccia zone	N A	100
<u>Deep strand:</u>					
179-33	1798.2	?	damage zone: microbreccia zones	52 [50-54]	56
181-34	1807.9	?	damage zone: microbreccia zones	38	64
183-14C	1815.9	?	damage zone: microbreccia zones	15	35
184-23	1821.9	?	damage zone: microbreccia zones	69	42

\*from LOCKNER *et al.* (2000) \*\*classification of OHTANI *et al.* (2000). N A = not attempted.

possible to “see” through the overprint of secondary mineralization to identify the primary igneous assemblage, because the low-temperature replacement reactions are typically pseudomorphic. Most of the samples are biotite-hornblende granodiorites, and a few are tonalites (Fig. 1; see also IKEDA, 2001 and TANAKA *et al.*, 2007). One K-feldspar



rich sample from the deep NIED fault strand has a granitic composition; a second deep NIED sample not included in Figure 1 probably also is a granite. Leaving out the granite outlier, the average igneous mode is 45% plagioclase, 33% quartz, 9% K-feldspar, 9%



Figure 3

(a) First-stage calcite (C) vein with crack-seal textures indicating multiple stages of alternating fracturing and secondary-mineral crystallization. The outermost, dark band on top is second-stage, brownish-yellow siderite (S), and siderite-filled cracks also cross-cut this vein (crossed polarizers; NIED 76-17). (b) Close-up of a microbreccia zone (boundary fractures marked by arrows) from the deep NIED fault strand, whose original void spaces are filled with zoned rhombs of alternating ankerite (A) and siderite (S) (plane-polarized light; NIED 183-14C). (c) Secondary-electron SEM image of a dilational fracture in the completely brecciated sample from the intermediate NIED fault strand (NIED 85-15B). The fracture surface is lined with small crystals of stage 3 calcite.

biotite, and 4% hornblende. Subhedral, tabular plagioclase phenocrysts are as much as 6 mm long; anhedral K-feldspar crystals and clusters of anhedral quartz crystals commonly reach 5 mm in diameter. The largest amphiboles are about 1.8 mm long and 1.1 mm wide, and the largest biotites are 2.5 mm long and 2 mm wide.

The relative abundances of primary igneous and low-temperature secondary minerals in the country rock and all but two of the damage-zone samples were estimated from a second set of point counts (Table 1), in which the percentage of secondary minerals comprises those that replace igneous minerals plus those that fill fractures and voids. No attempt was made to obtain counts of the mineral assemblages of the gouge or of two heavily brecciated samples (Table 1), and fragments too small to be identified using a petrographic microscope were not included in the counts that were made. Four samples (GSJ 101-2 and NIED 34-27, 82-40, and 179-33B) contain a sufficiently large number of uncounted small grains to potentially affect the reported secondary-mineral percentages. Error estimates for these four samples were made by calculating the effect on the percentages if all uncounted points were either igneous or secondary minerals (Table 1).

Secondary-mineral contents range from about 5% in a country rock sample to nearly 70% in one of the samples from the deep NIED fault strand (Table 1). Hornblende is the most readily altered mineral in the granodiorite. Relict amphiboles were found in only three samples, the two country-rock samples and the footwall sample GSJ 118-21, which shows relatively few effects of faulting (Table 1). The hornblende is pseudomorphically replaced by fine-grained aggregates of siderite and a montmorillonitic smectite clay. Using bulk X-ray diffraction techniques, OHTANI *et al.* (2000) identified smectite clays in much of the core from the GSJ drillhole. Biotite is better preserved than hornblende, but it commonly contains lozenges of laumontite or siderite along the cleavage planes. Some biotite is altered to pale-colored kaolinite, which was also identified by MATSUDA *et al.* (2004) in the NIED drillhole from XRD analysis. Other biotite is partly replaced by the smectite clay. Plagioclase is the more reactive feldspar, being replaced principally by laumontite but also by carbonate minerals. Quartz and K-feldspar are well preserved; low-temperature secondary minerals in these crystals typically fill fractures rather than replace the minerals. Flame perthite and myrmekite-like exsolution textures in K-feldspar may be faulting-induced deformation features (e.g., MOORE, 1987, 1990).

Carbonates are widespread fracture-filling and alteration minerals in the Nojima fault zone, and the type of carbonate mineral that crystallized has varied with time (Figs. 2–3) (MOORE *et al.*, 2000). The fracture-filling sequence comprises: 1) An early stage of calcite

coeval with laumontite (Figs. 2, 3a); 2) an extensive intermediate stage of siderite + ankerite (iron-rich dolomite; Figs. 2, 3b); and 3) late-stage calcite deposition in still-open fractures (Figs. 2, 3c) associated with trace amounts of barite. The transition between stages 1 and 2 is marked by co-crystallization of calcite and siderite, without laumontite. Alteration of mafic minerals may have provided most of the Fe and Mg for siderite and ankerite crystallization. This sequence was established from cross-cutting relationships. The laumontite  $\pm$  calcite veins are commonly cut by veins of siderite and/or ankerite, but do not themselves cross-cut any other veins. Stage 3 calcite-bearing fractures cross-cut all other structures. Three of the six samples in which the late-stage calcite was identified are fault gouge, one from each of the three gouge-bearing fault strands (GSJ 99-4 and NIED 45-23 and 81-22A). Present-day calcite deposits formed on a borehole seismometer that was deployed near the base of the GSJ drillhole for a year beginning in March, 2003 (FUJIMOTO *et al.*, 2007). Each of the first two stages comprises several episodes of crystallization, as indicated by features such as the crack-seal calcite vein in Figure 3a and the alternating concentric layers of siderite and ankerite in Figure 3b. Only a single episode of late calcite growth was seen in each of its occurrences.

#### 4.2. Brittle Microstructures

The degree of disruption of the damage-zone samples ranges from minor fracturing to complete fragmentation. Minor shear bands and wider shear zones overprint some of the heavily fractured and brecciated areas. Microstructures are described in the order of increasing deformation intensity below.

*Microfractures:* In mildly deformed granitic rock crack densities are typically greater in quartz than in feldspars (e.g., MORROW *et al.*, 1994; MOORE and LOCKNER, 1995), and this is also true for the Nojima granodiorite. Although the cracks can have any orientation, particularly in the vicinity of biotite, typically a set of elongate sub-parallel fractures dominates in quartz-rich areas, and a somewhat less prominent set of fractures is oriented at a large angle (60–90°) to the first (Fig. 4a). These two crack sets have the same orientations as older, healed cracks in quartz that are preserved as fluid-inclusion trails. Some of the microfractures associated with the Quaternary faulting have refractured portions of the healed cracks. On average, microfracture orientations in the feldspars are similar to those in the quartz, although the scatter is greater due to the influence of the two good cleavages in both feldspars.

Many individual microcracks are intragranular, transgranular, or grain-boundary cracks  $\leq 5$  mm in length (Fig. 4a). Longer, commonly mineral-lined intergranular fractures form as a result of the linkage of shorter cracks. Fractures in the less deformed damage-zone samples are generally  $\leq 0.04$  mm wide, and the majority are hairline cracks (e.g., Fig. 4a). Some relatively narrow fractures are lined with multiple rows of euhedral crystals (Fig. 4b). Most of the mineral-filled fractures or veins in the heavily deformed samples are also narrow, although a few are significantly wider, up to 3.6 mm for

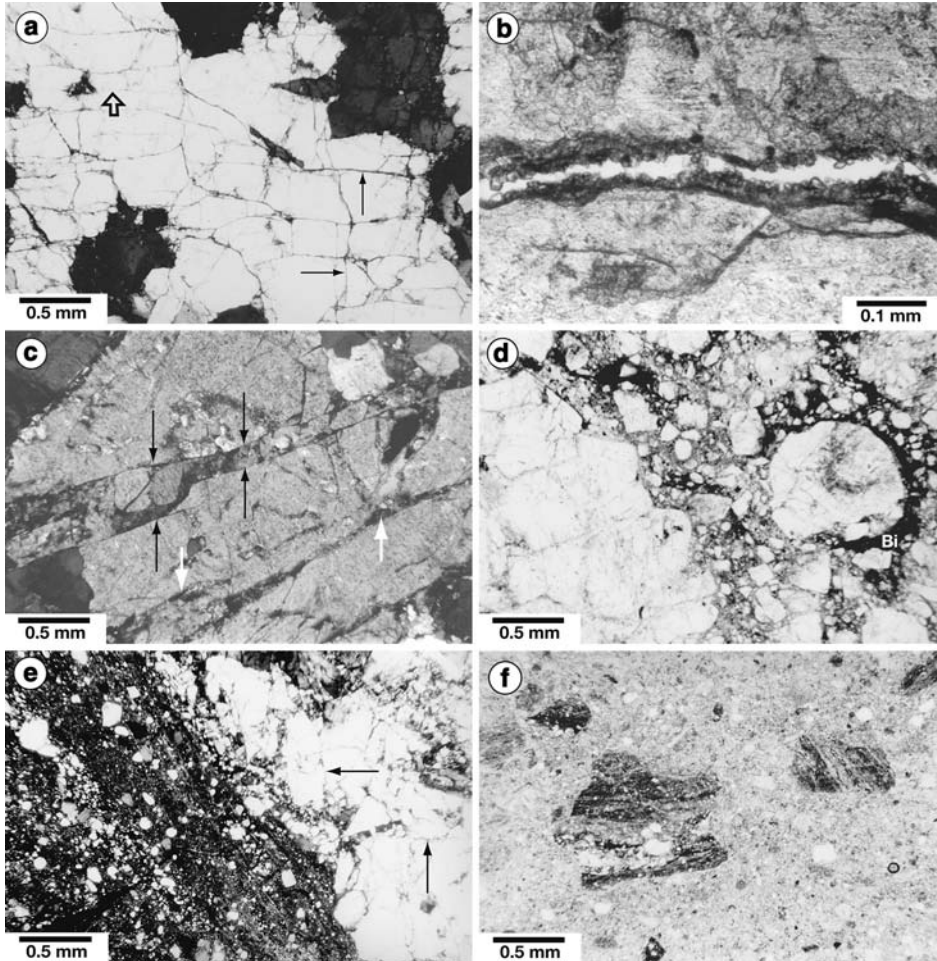


Figure 4

Photomicrographs illustrating the range of deformation textures in the samples. (a) Fractures in quartz form two, nearly perpendicular sets (examples indicated by long arrows), with the set trending left-to-right being the more prominent one. The quartz also contains older, healed fractures (the short, wide arrow points to one) preserved as fluid inclusion trails, with orientations similar to those of the more recent fractures (crossed polarizers; GSJ 118-21). (b) Open fracture lined with multiple rows of euhedral siderite crystals (plane-polarized light; GSJ 74-17). (c) Microbreccia zone in a plagioclase phenocryst. The pairs of black arrows indicate the change in width of the microbreccia zone where the boundary steps over to another microfracture. The plagioclase surrounding the microbreccia zone is undeformed except for a few mineral-filled fractures (marked by white arrows) (crossed polarizers; NIED 181-34). (d) Thoroughly disaggregated granodiorite within a 20-mm wide microbreccia zone. Biotite (Bi) wraps around variably sized, angular fragments of quartz and feldspar (plane-polarized light; NIED 76-17). (e) Boundary between a 6-mm wide minor shear band (left) and fractured damage-zone rock (right). The two principal fracture sets in the damage-zone rock (marked by arrows) are at moderate angles to the slip surface (see Fig. 8). The granodiorite within the shear is finely ground, and many of the larger grains have rounded rather than angular shapes. Alternating finer and coarser-grained bands define a foliation parallel to the shear planes (crossed polarizers; GSJ 101-2). (f) Gouge from the shallow NIED fault strand contains clasts of dark, foliated gouge, suggesting multiple episodes of shear and granulation (plane polarized light; NIED 45-23).

laumontite-filled veins and 1.5 mm for carbonate veins. The wider veins record multiple episodes of fracturing and sealing, as illustrated in Figure 3a. The orientation of the most prominent veins in a thin section usually corresponds to that of the dominant set of fractures in quartz, with some variability resulting from the way shorter cracks became linked to form them. Rough estimates of the amount of extension in the three most heavily veined thin sections were made by summing the vein widths along traverses parallel to the principal extension direction. The traverses yielded local extensional strains of 9% (NIED 43-37-1), 12.5% (NIED 32-20) and 15% (NIED 184-23).

*Microbreccia Zones:* The dominant features of the more highly deformed damage zone samples are microbreccia zones in which the rock between closely spaced fractures has been fragmented (Fig. 4c). Microbreccia zones can form from either set of microcracks, although the larger zones are usually parallel to the dominant set. Microbreccia zones as wide as 20 mm were identified (Table 1), and one sample (NIED 85-15B) is entirely microbreccia. Different stages of microbreccia zone development were identified in different thin sections. For example, the width of the microbreccia zone in Figure 4c doubles where it steps over to the next closest fracture, hence the wider microbreccia zones represent brecciation across an array of closely spaced fractures. Microbreccia zones extend their lengths by means of linkages to nearby zones in the same way that individual long fractures are formed. This is well illustrated by a composite microbreccia zone from the deep NIED strand that is up to 5 mm in width and extends the length of the thin section (Fig. 5a). Fracture spacing varies across the width of this zone, and the slivers of granodiorite between them are fragmented to varying degrees. Subsidiary microbreccia zones can form between pairs of cross fractures in the larger zones, as seen in the center of Figure 5a (white arrows).

The fragmented granodiorite within the wider microbreccia zones resembles a coarse-grained gouge (Fig. 4d), with fragments ranging from  $\approx 8$  mm in diameter down to clay size. Grain-size reduction in the microbreccia zones appears to be principally the product of intense dilational fracturing, such that the original distribution of igneous minerals in the brecciated regions can often be discerned. Many of the pore spaces in the microbreccia zones have been filled with secondary minerals (Fig. 6a). Fragments of quartz and feldspar have euhedral overgrowths, and neoblasts of these crystals fill pore spaces. Many plagioclase fragments have been partly albitized, and newly crystallized plagioclase is albite. Zeolites, carbonate minerals (e.g., Fig. 3b), and clay minerals are also common pore-filling secondary minerals.

Granodiorite adjacent to some of the larger microbreccia zones is strongly fractured and locally brecciated, particularly near intersecting microbreccia zones. For example, the sample containing the 20-mm wide microbreccia zone also has a second, nearly perpendicular zone on one side that is  $\geq 1.5$  mm wide. Biotites in the granodiorite bounded by these two zones have been heavily deformed and altered to siderite and clays. Large quartz and feldspar grains between the deformed biotites have been pulled apart along the two main fracturing directions, and the fractures are filled with siderite with crack-seal textures. Large void spaces partly filled with siderite are also present. On the

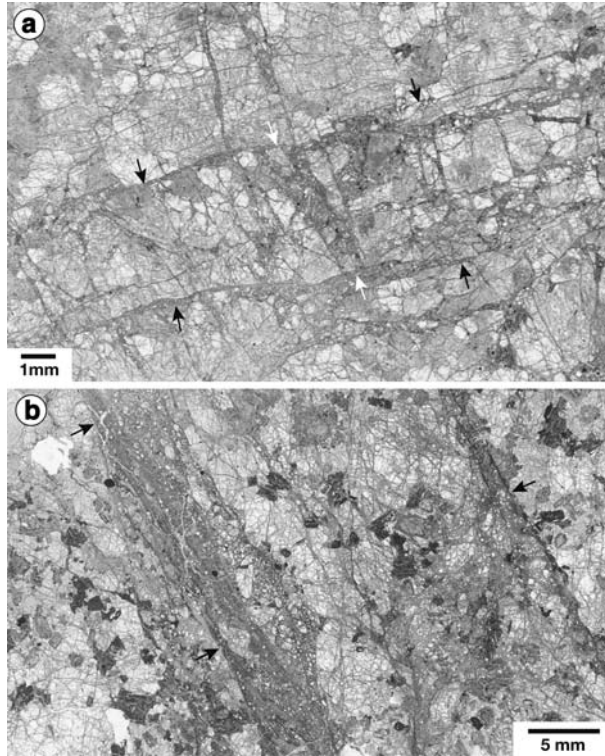


Figure 5

Views of larger structures from scans of thin sections. (a) Larger-scale microbreccia zone (NIED 183-14C); (b) Heavily damaged area between two minor shears (GSJ 101-2). Black arrows denote the borders of the zones; white arrows in (a) mark a band of concentrated fracturing between two cross fractures in the microbreccia zone.

other side of the large microbreccia zone, where the perpendicular microbreccia zone is not present, the granodiorite is less heavily fractured and biotite shows little replacement by carbonate minerals and clays.

The heavily deformed granodiorite in the GSJ fault strand and the shallow and intermediate NIED fault strands typically contain open fractures and open voids in brecciated areas. In contrast, the deep NIED fault strand contains few open fractures. Fractures in samples from that strand have been sealed with laumontite or carbonate minerals, and nearly all the void space in the microbreccia zones is filled (Fig. 3b).

*Minor Shear Bands:* Some of the samples located within 2-m horizontal distance of a gouge core contain minor shear bands (Table 1). The grains in the shear bands are much more strongly comminuted and typically more rounded than those in the microbreccia zones. In sample GSJ 101-2 (Fig. 4e) bands of alternating coarser and finer grained material are oriented roughly parallel to the strike of a given slip surface. The transitions between the well-developed shear bands and the adjoining rock in this sample are sharp,

Figure 6

Backscattered-electron SEM images. (a) Void space in a microbreccia zone is largely filled with euhedral, secondary K-feldspar (probably adularia, labelled K), albite (Ab), and interstitial montmorillonite (M). Some K-feldspar crystals show two stages of growth; the boundary between stages in one crystal is marked by arrows. Anhedral feldspars around the edges of the photo are partly altered breccia fragments (GSJ 91-6). (b) Clast of pseudotachylyte from the shallow NIED fault strand, characterized by round pores and partly resorbed quartz crystals (Q) in a light-gray, cryptocrystalline matrix. Possible euhedral crystallites now contain calcite (C) and montmorillonite (M) (NIED 45-23). (c) Closer view of the fine-grained gouge in (b), with a clast of gouge (G) in the center. Many quartz (Q) grains are present in this view, along with K-feldspar (K), ankerite (A), and albite (Ab) (NIED 45-23).

and the shear-band orientations roughly bisect the trends of the perpendicular sets of fractures and microbreccias. The 4-mm wide shear band shown in Figure 4e contains clasts of foliated rock, suggesting multiple episodes of slip. Offset across the wider shear bands could not be determined; however, a narrow shear in sample NIED 43-37-1 offsets separate ankerite and laumontite veins 9 mm right-laterally. This shear band varies in texture from a 0.3-mm wide band that is very fine-grained but not well foliated to a wider but more diffuse zone. No evidence for more than one episode of slip was found in this shear band. Two other relatively fine-grained bands that cut across microbreccia zones may be incipient shear bands.

The 4-mm wide shear band and a second, less well defined one bound a roughly 10-mm wide sliver of granodiorite that is more heavily broken up than the rock outside the area between the two shear bands (Fig. 5b). The overall structure is interpreted as a minor shear zone.

*Fault Gouge:* The approximately 30-cm thick gouge core identified in the GSJ drillhole is divided into three subzones that were active at different times (FUJIMOTO *et al.*, 2000; OHTANI *et al.*, 2000): the Type I and Type II subzones are the locations of former principal slip surfaces, whereas the Type III gouge is inferred to have taken up the offset during the 1995 earthquake. The four gouge samples that we obtained from the GSJ and NIED drillholes correspond to the older, Type I and Type II subzones:

- Type I — GSJ 98-31 and NIED 81-22a (intermediate strand, Fig. 2 of paper I).
- Type II — GSJ 99-4 and NIED 45-23 (shallow strand).

The Type I GSJ sample is a coarse-grained, foliated gouge that is cross-cut by a network of fractures filled with either the early laumontite + calcite or the subsequent siderite + ankerite mineral assemblages. These textures suggest that this gouge sublayer has long been abandoned as a site of localized shear and now behaves as part of the damage zone (see also BOULLIER *et al.*, 2004). The gouge sample from the intermediate NIED fault strand is a coarse-grained, foliated gouge that has some textural similarities to the Type I GSJ gouge sample and that also is cut by laumontite-lined fractures.

The Type II GSJ gouge and the gouge sample from the shallow NIED fault strand (Fig. 4f) are very similar, fine-grained, massive gouges that contain fragments of earlier-formed, foliated gouge (Fig. 4f), indicating multiple episodes of localized shear. The foliation within these clasts of gouge is similar to that seen in the minor shear bands



Figure 7

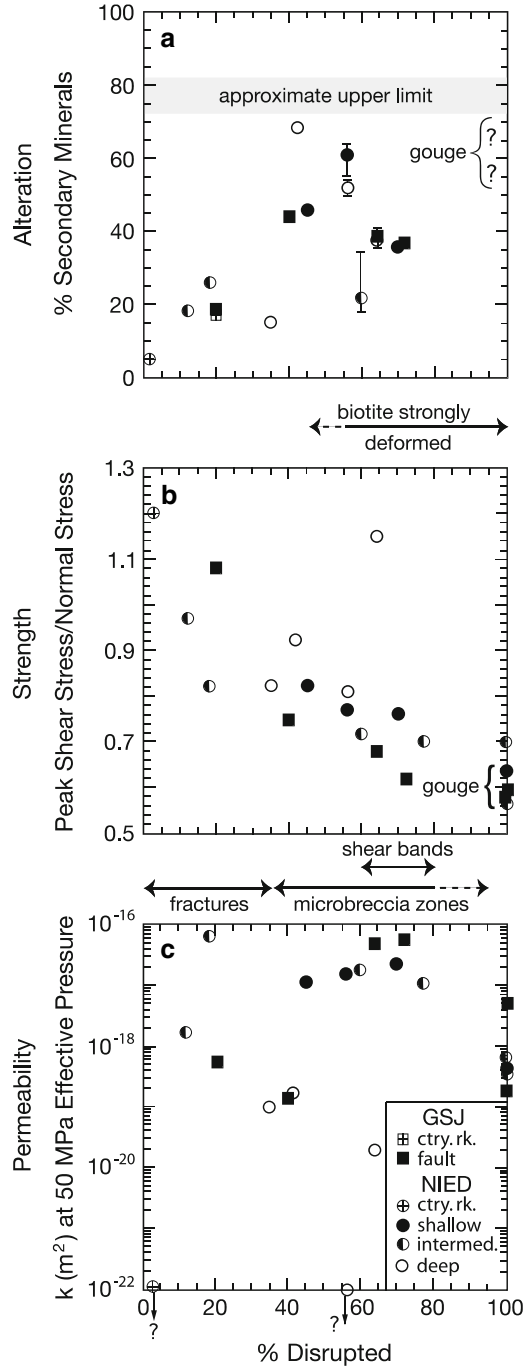
Comparison of the degree of deformation of a given sample with its: (a) secondary-mineral content (degree of alteration), (b) peak shear strength, and (c) permeability ( $k$ ); reported laboratory data were measured at 50 MPa effective pressure. In (a), error bars were added to the four samples for which small to significant numbers of unidentifiable grains were not counted (Table 1). Quartz and K-feldspar are resistant to alteration in these samples, and an approximate upper limit to the proportion of secondary minerals in a given sample plotted in (a) would be determined by its original quartz + K-feldspar content, adjusted for the amount of dilation and infilling by secondary minerals. The secondary-mineral content of the gouge samples may approach the upper limit. Samples containing only dilational fractures were  $\leq 45\%$  deformed, and samples containing microbreccia zones were  $\geq 35\%$  deformed.

(Fig. 4e). FUJIMOTO *et al.* (2000) and OHTANI *et al.* (2000) described clasts of the  $\approx 56$  Ma (MURAKAMI and TAGAMI, 2004) pseudotachylyte in the Type II GSJ gouge, and we found a similar clast in the gouge layer of the shallow NIED fault strand (Fig. 6b; compare with Fig. 3f of FUJIMOTO *et al.*, 2000, p. 108). TANAKA *et al.* (2007) also reported clasts of pseudotachylyte in an ultracataclasite subzone that is cut by younger shears in the core of the shallow NIED strand. Many grains of quartz, K-feldspar, unaltered and albitized plagioclase, laumontite, calcite, ankerite, and siderite were identified in the fine-grained gouge samples with the SEM (e.g., Fig. 6c). The abundance of siderite and ankerite occurring as clasts in the gouge suggests that these two fine-grained gouge samples were sheared considerably more recently than was the type I gouge. Both gouge samples, however, do contain late-stage calcite  $\pm$  barite-lined fractures.

#### 4.3. Deformation Intensity

Deformation intensity was estimated from the degree of disruption of each sample, determined by a point count of “intact” versus “disrupted” granite, in which the “disrupted” counts comprise open and filled microfractures, microbreccia zones, and minor shear bands (Table 1). This method provides a simple way to assess and compare the cumulative damage in different granodiorite samples, and the reported percentages represent the total damage of various types incurred during the faulting history. In gouge, the deformation processes resulted in the complete disaggregation of the rock, and all such samples were assigned a value of 100% disrupted. The large microbreccia zone that constitutes all of sample NIED 85-15B (Table 1) is also considered 100% disrupted. All of the samples in Table 1 that are listed as  $< 100\%$  disrupted contain at least some areas of relatively intact igneous rock. These counts represent the deformation intensity at the scale of the thin sections and the tested laboratory samples.

The percentage of secondary minerals in a sample (Table 1) is plotted against its degree of disruption in Figure 7a. Error bars are included for the four samples with small to significant numbers of unidentifiable, uncounted grains. In general, the abundance of secondary minerals increases with increasing deformation in country-rock and damage-zone samples. Because quartz and K-feldspar are resistant to alteration in these samples, there will be some upper limit to the secondary-mineral content in a sample that is a function of its igneous mode (Fig. 1). The amount of secondary minerals will vary with



the amount of dilation of the sample and the degree to which the opened cracks and voids have been filled with secondary minerals. The degree of disruption of one sample from the deep NIED fault strand (NIED 184-23, Table 1) could not be determined because of the extensive alteration overprint, but its estimated 69% secondary-mineral content is probably near the limiting value. Most of the plagioclase and biotite and all of the hornblende in that sample have been altered, and the numerous wide laumontite veins indicate substantial extensional strain. The quartz is heavily fractured, and essentially all the fractures are filled, predominantly with minerals other than quartz. In contrast, the minor K-feldspar in the sample is only sparsely fractured and little altered. Gouge samples may also have secondary-mineral contents near the upper limit (Fig. 7a).

Relationships between degree of deformation and the strength and permeability data presented in paper I are shown in Figures 7b and 7c, respectively. The strength data plotted in Figure 7b are the peak strengths at 50 MPa effective confining pressure. With one marked exception, a strong inverse relationship exists between peak strength of a rock sample and its degree of disruption. The tested intact-rock sample is the strongest with a ratio of peak shear stress to normal stress of  $\approx 1.2$ , and the gouge-core samples are the weakest at  $\approx 0.56$ – $0.64$ . The exception to the trend in Figure 7b is a heavily deformed sample from the deep NIED fault strand whose peak strength nevertheless approaches that of the country rock. A correlation between permeability and degree of disruption (Fig. 7c) is weaker than that between peak strength and deformation intensity, nonetheless the relationship is more pronounced if the deep NIED samples are not considered. Compared to the country-rock sample, permeability is at least 3 orders of magnitude higher for all the GSJ and the shallow- and intermediate-strand NIED samples. With one exception, samples that are  $\leq 40\%$  disrupted have lower permeability than those in the range 40–80% disrupted. Permeability of the completely disaggregated samples is 1–2 orders of magnitude lower than that of the 40–80% disrupted samples. The samples from the deep NIED fault strand have lower permeabilities than all but one of the damage-zone samples from the other strands.

## 5. Discussion

### 5.1. Microstructure Orientations

Although the core samples were not oriented, the relative orientations of the different types of microstructures are consistent from sample to sample in the two boreholes; a representative example is shown in Figure 8. Summarizing the microstructural descriptions presented in previous sections, microfractures concentrated in quartz form at the lowest level of deformation in the Nojima fault, and two nearly perpendicular sets of fractures commonly can be identified, with one set dominating over the other. The widest veins and the largest microbreccia zones are oriented parallel to the dominant fracture set, whereas minor shears cross-cut both sets (Fig. 8).

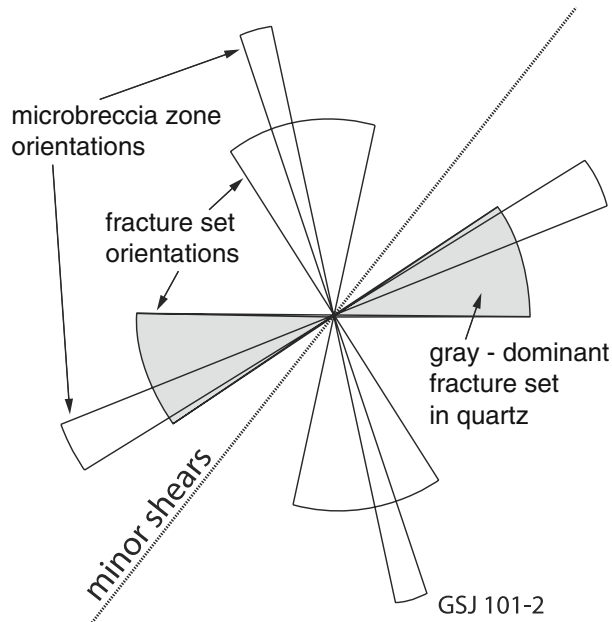


Figure 8

Relative strikes of microstructural elements in damage-zone sample GSJ 101-2. The figure was oriented such that the dominant fracture set in quartz has the roughly EW (to NE-SW) trend measured by TAKESHITA and YAGI (2000), and the minor shear is sub-parallel to the strike ( $\approx N36^\circ E$ ) of the Nojima fault (that is, a north arrow would point upwards in this interpretation).

CÉLÉRIER *et al.* (2000) determined that subsidiary shear planes identified in borehole televiewer images from the GSJ drillhole principally have NE-SW trending strikes, subparallel to the strike of the fault. TAKESHITA and YAGI (2000, 2001) measured the orientations of healed microcracks and cracks sealed with carbonate minerals in quartz in oriented core samples from the GSJ drillhole and from a second drillhole that crosses the Nojima fault near its southern end. The sealed fractures generally have the same orientations as the healed cracks, and they form three groups: one set of sub-horizontal fractures and two sets of vertical cracks oriented N-S (to NW-SE) and E-W (to NE-SW) (TAKESHITA and YAGI, 2000, 2001). Among the vertical microcracks, E-W orientations generally predominate for the sealed cracks and N-S orientations for the older, healed cracks. Mutually perpendicular, healed crack sets in quartz in plutonic rocks have been attributed to contraction of the quartz during cooling of the plutons (e.g., VOLLBRECHT *et al.*, 1991), and the prominence of the N-S vertical set was interpreted by TAKESHITA and YAGI (2000, 2001) to reflect N-S compression during solidification of the Nojima granodiorite. The dominance of E-W orientations among the carbonate-sealed vertical cracks is consistent with the E-W compression that dominated during the Quaternary (SENO, 1999).

The diagram in Figure 8 was rotated to a position in which the dominant set of fault-related microfractures in quartz would have the roughly E-W (to NE-SW) orientation determined by TAKESHITA and YAGI (2001). This positioning also causes the minor shear to be oriented subparallel to the strike of the Nojima fault, consistent with the results of CÉLÉRIER *et al.*, (2000). The arrangement of microstructures in Figure 8 looks the same if the figure is rotated 180°C; thus two possible matches exist for each thin section (see also MOORE *et al.*, 2001).

### 5.2. Microstructural Evolution

WONG (1982) described how long, closely spaced dilational fractures in quartz isolate narrow columns that buckle and fragment accompanying failure of granitic rock in laboratory loading experiments. KING and SAMMIS (1992) incorporated these and other observations into a model of shear-zone development and the formation of fault gouge. In their model, clustered dilational fractures that initiated from flaws in the rock expand their lengths, until the aspect ratio of the rock slivers between the fractures reaches a critical value beyond which the columns bend and then break along transverse, tensile fractures. This process, repeated at smaller and larger scales at clusters of dilational fractures, eventually produces localized zones of fragmented rock that KING and SAMMIS (1992) call 'superdefects'. Closely-spaced superdefects may interact and link together over time to form a shear band.

The KING and SAMMIS (1992) model provides a framework for interpreting the microstructural features of the core samples from the Nojima fault zone. In particular, the microbreccia zones correspond to their superdefects, and the sequence of development of the microbreccia zones, described previously, is essentially the same. Initial microbreccia zone lengths are on the order of a few millimeters, corresponding to the grain sizes of igneous feldspars and quartz (Fig. 4c). Some of them have scaled upwards by stepping across to adjoining fractures to increase width and by linking up with nearby zones to increase length (Fig. 5a). Downward scaling eventually leads to complete fragmentation of the rock within the zones (Fig. 4d). Initiation of the microbreccia zones occurs in rock that has been significantly affected by dilational fracturing. Formation of a minor shear band requires even greater amounts of disruption, which for this sample set is restricted to  $\leq 2$  m horizontal distance from the fault cores (Table 1). Once the shear bands form, deformation may be localized within them, so that the surrounding rock is not completely disrupted.

### 5.3. Physical Properties Relative to Microstructural Development

The interpretation of peak strength in terms of deformation intensity is straightforward, with strength decreasing continuously with increasing cumulative damage (Fig. 7b). The greatest strength decreases accompany the initial increases of fracture density, and the heavily deformed damage-zone rocks (>60% disrupted) are not

significantly stronger than the completely disaggregated microbreccia and gouge samples.

Shear strength reaches a minimum in the gouge core and the one completely brecciated damage-zone sample, but the coefficient of friction does not go below  $\approx 0.55$ . Such friction values are consistent with the abundance of hard grains such as quartz and feldspars in the gouge (Fig. 6c). Laumontite and calcite also are strong minerals at room temperature (MORROW and BYERLEE, 1991; MORROW *et al.*, 2000); other zeolites and carbonate minerals are likely to have similar strengths. These strong minerals are mixed with varying amounts of weaker clay minerals, although smectite clays will contribute more to the weakening than kaolinite (MOORE and LOCKNER, 2004).

Some of the implications of the shear-forming process that KING and SAMMIS (1992) outline are applicable to the permeability trends of these samples (Fig. 7c). Tensile cracking will dilate the rock, and the Nojima samples characterized by dilational fracturing alone have permeabilities at least 1-2 orders of magnitude greater than the country-rock permeability. However, the most permeable samples are principally those that contain microbreccia zones. Buckling and rotation of narrow rock columns between adjoining fractures will initially generate large fragments that rotate and create additional void space in the microbreccia zones. Continued fracturing at smaller scales in the developing microbreccia zones will gradually reduce the grain size of the breccia, leading to greater compaction and consequently a reduction of porosity and permeability in the zones. The smaller microbreccia zones with relatively large fragments have substantial voids that serve as permeability conduits. The larger microbreccia zones and especially the minor shear bands are characterized by finer-grained, more densely packed fragments. For the samples containing these structures, enhanced fracturing in the vicinity of intersecting microbreccia zones or between minor shear bands is the probable cause of their high net permeability values. A connected fracture network appears to be critical to maintaining elevated permeability, such that the completely brecciated sample has permeability comparable to that of the gouge samples. The gouge sample whose permeability is about an order of magnitude higher than that of the others (Fig. 7c) is the type I GSJ gouge sample (GSJ 98-31), which has been extensively fractured (see also BOULLIER *et al.*, 2004). The permeability measurements for that sample may thus be a reflection more of microfracture permeability than of matrix permeability.

As the secondary mineralization textures of these samples indicate, permeability of the granodiorite in the damage zone changes continually, as dilational fracturing processes accompanying earthquakes create pathways for fluid flow that subsequently become clogged with newly precipitated minerals. Accordingly, the samples with the highest permeabilities also contain  $\approx 30\text{--}60\%$  secondary minerals (Fig. 7). Samples from the GSJ drillhole and the shallow and intermediate fault strands from the NIED drillhole characteristically contain fresh-looking dilational fractures and brecciated areas. In contrast, there is little evidence of recent fracturing in the samples from the deep NIED fault strand.

The deep NIED fault strand is characterized by permeability values that are closer to the country rock than to the other three fault strands, and the strength of one of the three samples approaches that of the country rock (Figs. 7b-c). The textures in the examined samples from the deep NIED fault strand support the conclusion of LOCKNER *et al.* (paper D) that this strand is an older, abandoned fault trace. Deformation largely ceased during the early laumontite-forming stage, but fluids continued to migrate through these rocks. As a result, nearly all the pore spaces in the microbreccia zones have been filled and most fractures are sealed. Unless active fracturing continues to create new void space, permeability will gradually decrease. In these samples from the deep NIED strand, permeability is returning to the original values of the granodiorite country rock more readily than strength is restored (Fig. 7). This implies that a sealed fracture or a cemented microbreccia zone is not particularly strong, as also illustrated by the crack-seal veins that have repeatedly fractured along the vein walls. Refracturing of some of the older microfractures in quartz suggests that even healed cracks are not as strong as the original quartz grains.

## 6. Concluding Remarks

Core samples obtained from deep drillholes that cross the active Nojima fault of Japan provide important new information about fault-zone processes in crystalline rock. This petrographic study has presented some general aspects of the microstructural evolution of the damage zone and the effects that the microstructures have on physical properties such as permeability and strength. Offset is concentrated within the core of a strand, although minor sheared zones are present in damage-zone rocks immediately adjacent to the fault cores. Deformation in the damage zone is largely the result of brittle fracturing processes that, at their peak, produce wide microbreccia zones and associated intensely fractured rocks. Fractures and pore spaces are partly filled with secondary minerals deposited from migrating solutions that have also partly altered the igneous mafic minerals and plagioclase. This scenario is consistent with the model of fault zone architecture and the systematic variations in fault-zone properties and processes over the seismic cycle described by CHESTER *et al.* (1993) from detailed observations of the San Gabriel and Punchbowl faults. The measured strength and permeability data for the core samples thus represent just one moment in a continually evolving system. Abandonment of a fault strand is accompanied by a gradual return of permeability and strength towards the country-rock values, although permeability recovers more readily than strength, and strength may never attain the original value.

The nearly continuous core from the GSJ and NIED drillholes is an extremely valuable resource for understanding the deformational and mineralogical evolution of a fault zone. The fault has not experienced considerable offset and the fault-zone geometry is reasonably simple. The deep NIED fault strand in particular is a critical source of

information on the early stages of microstructural development of the fault zone that can be used to interpret the more heavily deformed rocks associated with the active fault strands.

## REFERENCES

- AWATA, Y., and SUZUKI, Y. (1996), *Paleoseismology and activity study of the Nojima fault system, which generated the Hyogo-ken Nanbu earthquake of January 17, 1995*, Geol. Surv. Japan Open-File Report 250, 4–8 (in Japanese).
- AWATA, Y., MIZUNO, K., SUGIYAMA, Y., IMURA, R., SHIMOKAWA, K., OKUMURA, K., and TSUKUDA, E. (1996), *Surface fault ruptures on the northwest coast of Awaji Island associated with the Hyogoken Nanbu earthquake of 1995*, J. Seismol. Soc. Japan 49, 113–124 (in Japanese with English abstract).
- BOULLIER, A.-M., FUJIMOTO, K., OHTANI, T., ROMAN-ROSS, G., LEWIN, E., ITO, H., PEZARD, P., and IDLEFONSE, B. (2004), *Textural evidence for recent co-seismic circulation of fluids in the Nojima fault zone, Awaji island, Japan*, Tectonophysics 378, 165–181.
- CAINE, J.S., EVANS, J.P., and FORSTER, C.B. (1996), *Fault zone architecture and permeability structure*, Geology 24, 1025–1028.
- CÉLÉRIER, B.P., PEZARD, P.A., ITO, H., and KIGUCHI, T. (2000), *Borehole wall geometry across the Nojima fault: BHTV acoustic scans analysis from the GSJ Hirabayashi hole, Japan*. In *The International Workshop on the Nojima Fault Core and Borehole Data Analysis* (eds. Ito, H., Fujimoto, K., Tanaka, H., and Lockner, D.), U. S. Geol. Surv. Open-File Report 00-129, pp. 233–238.
- CHESTER, F.M., and LOGAN, J.M. (1986), *Implications for mechanical properties of brittle faults from observations of the Punchbowl fault zone, California*. In *Internal Structure of Fault Zones* (ed. Wang, C.-Y.), Pure Appl. Geophys. 124, 79–106.
- CHESTER, F.M., EVANS, J.P., and BIEGEL, R.L. (1993), *Internal structure and weakening mechanisms of the San Andreas fault*, J. Geophys. Res. 98, 771–786.
- FUJIMOTO, K., TANAKA, H., TOMIDA, N., OHTANI, T., and ITO, H. (2000), *Characterization of fault gouge from GSJ Hirabayashi core samples and implications for the activity of the Nojima fault*. In *The International Workshop on the Nojima Fault Core and Borehole Data Analysis* (eds. Ito, H., Fujimoto, K., Tanaka, H., and Lockner, D.), U. S. Geol. Surv. Open-File Report 00-129, pp. 103–109.
- FUJIMOTO, K., UEDA, A., OHTANI, T., TAKAHASHI, M., ITO, H., TANAKA, H., and BOULLIER, A.-M. (2007), *Borehole water and hydrologic model around the Nojima fault, SW Japan*, Tectonophysics 443, 174–182.
- IKEDA, R. (2001), *Outline of the fault zone drilling project by NIED in the vicinity of the 1995 Hyogo-ken Nanbu earthquake, Japan*, Island Arc 10, 199–205.
- IKEDA, R., IIO, Y., and OMURA, K. (2001), *In situ stress measurements in NIED boreholes in and around the fault zone near the 1995 Hyogo-ken Nanbu earthquake, Japan*, Island Arc 10, 252–260.
- KING, G.C.P., and SAMMIS, C.G. (1992), *The mechanics of finite brittle strain*, Pure Appl. Geophys. 138, 611–640.
- LIN, A., and UDA, S. (1996), *Morphological characteristics of the earthquake surface rupture which occurred on Awaji Island, associated with the 1995 southern Hyogo Prefecture earthquake*, Island Arc 5, 1–5.
- LIN, A., SHIMAMOTO, T., MARUYAMA, T., SIGETOMI, M., MIYATA, T., TAKEMURA, K., TANAKA, H., UDA, S., and MURATA, A. (2001), *Comparative study of cataclastic rocks from a drill core and outcrops of the Nojima Fault zone on Awaji Island, Japan*, Island Arc 10, 368–380.
- LOCKNER, D., NAKA, H., TANAKA, H., ITO, H., IKEDA, R., and OMURA, K. (2009), *Geometry of the Nojima fault at Nojima-Hirabayashi, Japan – I. A simple damage structure inferred from borehole core permeability*, this volume.
- MATSUDA, T., OMURA, K., IKEDA, R., ARAI, T., KOBAYASHI, K., SHIMADA, K., TANAKA, H., TOMITA, T., and HIRANO, S. (2004), *Fracture-zone conditions on a recently active fault: Insights from mineralogical and geochemical analyses of the Hirabayashi NIED drill core on the Nojima fault, southwest Japan, which ruptured in the 1995 Kobe earthquake*, Tectonophysics 378, 143–163.
- MIZUNO, K., HATTORI, H., SANGAWA, A., and TAKAHASHI, Y. (1990), *Geology of the Akashi district, quadrangle series*, Geol. Surv. Japan, scale 1:50,000, 90 pp. (in Japanese with English abstract).

- MOORE, D.E. (1987), *Syndeformational metamorphic myrmekite in granodiorite of the Sierra Nevada, California*, Geol. Soc. Am. Abstr. with Progr. 19(7), 776.
- MOORE, D.E. (1990), *Flame perthite associated with faulting in granodiorite, Mt. Abbot quadrangle, California*, EOS, Trans. Am. Geophys. Union 71, 1596.
- MOORE, D.E., and LOCKNER, D.A. (1995), *The role of microcracking in shear-fracture propagation in granite*, J. Struct. Geol. 17, 95–114.
- MOORE, D.E., and LOCKNER, D.A. (2004), *Crystallographic controls on the frictional behavior of dry and water-saturated sheet structure minerals*, J. Geophys. Res. 109, B03401, doi: [10.1029/2003JB002582](https://doi.org/10.1029/2003JB002582).
- MOORE, D.E., HICKMAN, S., LOCKNER, D.A., and DOBSON, P.F. (2001), *Hydrothermal minerals and microstructures in the Silangkitang geothermal field along the Great Sumatran fault zone, Sumatra*, Geol. Soc. Am. Bull. 113, 1179–1192.
- MOORE, D.E., LOCKNER, D.A., ITO, H., and IKEDA, R. (2000), *Carbonate mineralization sequence and the earthquake history of the Nojima fault zone, Japan*, EOS, Trans. Am. Geophys. Union 81, F1099–F1100.
- MORROW, C.A., and BYERLEE, J.D. (1991), *A note on the frictional strength of laumontite from Cajon Pass, California*, Geophys. Res. Lett. 18, 211–214.
- MORROW, C., LOCKNER, D., HICKMAN, S., RUSANOV, M., and RÖCKEL, T. (1994), *Effects of lithology and depth on the permeability of core samples from the Kola and KTB drill holes*, J. Geophys. Res. 99, 7263–7274.
- MORROW, C.A., MOORE, D.E., and LOCKNER, D.A. (2000), *The effect of mineral bond strength and adsorbed water on fault gouge frictional strength*, Geophys. Res. Lett. 27, 815–818.
- MURAKAMI, M., and TAGAMI, T. (2004), *Dating pseudotachylite of the Nojima fault using the zircon fission-track method*, Geophys. Res. Lett. 31, L12604, doi:[10.1029/2004GL020211](https://doi.org/10.1029/2004GL020211).
- MURATA, A., TAKEMURA, K., MIYATA, T., and LIN, A. (2001), *Quaternary vertical offset and average slip rate of the Nojima Fault on Awaji Island, Japan*, Island Arc 10, 360–367.
- OHTANI, T., FUJIMOTO, K., ITO, H., TANAKA, H., TOMIDA, N., and HIGUCHI, T. (2000), *Fault rocks and past to recent fluid characteristics from the borehole survey of the Nojima fault ruptured in the 1995 Kobe earthquake, southwest Japan*, J. Geophys. Res. 105, 16,161–16,171.
- OTSUKI, K., MONZAWA, N., and NAGASE, T. (2003), *Fluidization and melting of fault gouge during seismic slip: Identification in the Nojima fault zone and implications for focal earthquake mechanisms*, J. Geophys. Res. 108, B4, 2192, doi:[10.1029/2001JB001711](https://doi.org/10.1029/2001JB001711).
- SENO, T. (1999), *Syntheses of the regional stress field of the Japanese islands*, Island Arc 8, 66–79.
- STRECKEISEN, A. (1974), *Classification and nomenclature of plutonic rocks*, Geol. Rundschau 63, 773–785.
- TAGAMI, T., and MURAKAMI, M. (2007), *Probing fault zone heterogeneity on the Nojima fault: Constraints from zircon fission-track analysis of borehole samples*, Tectonophysics 443, 139–152.
- TAKAHASHI, Y. (1992), *K-Ar ages of the granitic rocks in Awaji Island — with an emphasis on timing of mylonitization*, Gankou 87, 291–299 (in Japanese with English abstract).
- TAKESHITA, T., and YAGI, K. (2000), *Dynamic analysis based on 3-D orientation distribution of microcracks in quartz from the Cretaceous granodiorite core samples drilled along the Nojima fault, southwest Japan*. In *The International Workshop on the Nojima Fault Core and Borehole Data Analysis* (eds. Ito, H., Fujimoto, K., Tanaka, H., and Lockner, D.), U. S. Geol. Surv. Open-File Report 00-129, pp. 133–140.
- TAKESHITA, T., and YAGI, K. (2001), *Paleostress orientation from 3-D orientation distribution of microcracks in quartz from the Cretaceous granodiorite core samples drilled through the Nojima fault, southwest Japan*, Island Arc 10, 495–505.
- TANAKA, H., FUJIMOTO, K., OHTANI, T., and ITO, H. (2001), *Structural and chemical characterization of shear zones in the freshly activated Nojima fault, Awaji Island, southwest Japan*, J. Geophys. Res. 106, 8789–8810.
- TANAKA, H., OMURA, K., MATSUDA, T., IKEDA, R., KOBAYASHI, K., MURAKAMI, M., and SHIMADA, K. (2007), *Architectural evolution of the Nojima fault and identification of the activated slip layer by Kobe earthquake*, J. Geophys. Res. 112, B07304, doi:[10.1029/2005JB003977](https://doi.org/10.1029/2005JB003977).
- VOLLBRECHT, A., RUST, S., and WEBER, K. (1991), *Development of microcracks in granites during cooling and uplift: Examples from the Variscan basement in NE Bavaria, Germany*, J. Struct. Geol. 13, 787–799.
- WONG, T.-F. (1982), *Micromechanics of faulting in Westerly granite*, Int. J. Rock Mech. Mining Sci. Geomech. Abstr. 19, 49–64.

YAMAMOTO, K., SATO, N., and YABE, Y. (2000), *Stress state around the Nojima fault estimated from core measurements*. In *The International Workshop on the Nojima Fault Core and Borehole Data Analysis* (eds. Ito, H., Fujimoto, K., Tanaka, H., and Lockner, D.), U. S. Geol. Surv. Open-File Report 00-129, pp. 239–246.

(Received September 29, 2008, revised March 6, 2009)

Published Online First: June 30, 2009

---

To access this journal online:  
[www.birkhauser.ch/pageoph](http://www.birkhauser.ch/pageoph)

---